JACS
JOURNAL OF THE AMERICAN CHEMICAL SOCIETY

ARTICLE

pubs.acs.org/JACS

Coherent Nuclear Dynamics in Ultrafast Photoinduced Structural Change of Bis(diimine)copper(I) Complex

Munetaka Iwamura,[†] Hidekazu Watanabe,[‡] Kunihiko Ishii, Satoshi Takeuchi, and Tahei Tahara*

Molecular Spectroscopy Laboratory, Advanced Science Institute (ASI), RIKEN, 2-1 Hirosawa, Wako, Saitama 351-0198, Japan

Supporting Information

ABSTRACT: The photoinduced structural change of a prototype metal complex, $[Cu(dmphen)_2]^+$ (dmphen = 2,9-dimethyl-1,10-phenanthroline), was studied by ultrafast spectroscopy with time resolution as high as 30 fs. Time-resolved absorption measured with direct S_1 excitation clearly showed spectral changes attributable to the D_{2d} (perpendicular) → D_2 (flattened) structural change occurring in the metal-to-ligand charge transfer singlet excited state (^{1}MLCT) and the subsequent S_1 → T_1 intersystem crossing. It was confirmed that the two processes occur with time constants of ∼0.8 ps (structural change) and ∼10 ps (intersystem crossing), and their time scales are clearly well-separated. A distinct oscillation of the transient absorption signal was observed in the femtosecond region, which arises from the coherent nuclear motion of the perpendicular S_1 state that was directly generated by photoexcitation. This demonstrated that the perpendicular S_1 state has a well-defined vibrational structure and can vibrate within its subpicosecond lifetime. In other words, the S_1 state stays undistorted in a short period, and the coherent nuclear motion is maintained in this state. Time-dependent density functional theory (TDDFT) calculations gave consistent results, indicating a very flat feature and even a local minimum at the perpendicular structure on the S_1 potential energy surface. The vibrational assignments of the S_1 nuclear wavepacket motion were made on the basis of the TDDFT calculation. It was concluded that photoexcitation induces a_1 vibrations containing the Cu−ligand bond length change and a b_1 vibration attributed to the ligand-twisting motion that has the same symmetry as the flattening distortion. Ultrafast spectroscopy and complementary quantum chemical calculation provided an overall picture and new understanding of the photoinduced structural change of the prototypical metal complex.

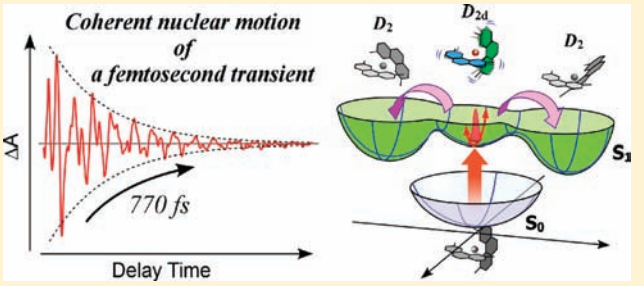

INTRODUCTION

Transition metal complexes have unique electronic and magnetic properties[1] and play important roles in various biological systems and applications. Especially, photochemistry of transition metal complexes attracts much interest in the field of solar energy conversion and optoelectronic devices.[2,3] In spite of its importance, however, the primary photochemical process of the metal complexes has not been well clarified so far because the excited-state dynamics of the metal complex is very fast and complicated, compared with that of ordinary organic compounds. It is only recently that advanced ultrafast spectroscopy in the optical and X-ray regions started disclosing the ultrafast processes of the metal complexes that occur in the femtosecond time region.[4−12] One of the key photochemical properties of metal complexes is the structural change induced by photoexcitation. As is well-known, the structure of the transition metal complexes directly reflects the configuration of d electrons, so that the excitation of the d electron often induces a substantial structural change. Because such a photoinduced structural change is an essential component of photophysics and photochemistry of metal complexes,[13] the relevant knowledge of the dynamics and mechanism is indispensable to understand the properties of metal complexes.[14−16] Furthermore, it is of fundamental importance to elucidate how the initial nuclear motion is correlated to the large structural change occurring afterward, since the relationship between the coherent nuclear motion and reaction is a central issue in the study of ultrafast photochemical reactions.[17−20] Although the excited-state nuclear wavepacket motion of several metal complexes has been observed very recently,[21−24] we do not have proper knowledge of its identification and relevance to the overall relaxation process of the metal complex.

Bis(2,9-dimethyl-1,10-phenanthroline)copper(I) ($[Cu(dmphen)_2]^+$; dmphen = 2,9-dimethyl-1,10-phenanthroline) is known as a prototypical metal complex that undergoes a large photoinduced structural change.[25−28] The electronic ground (S_0) state of $[Cu(dmphen)_2]^+$ has a D_{2d} structure where the two planar dimethylphenanthroline ligands are perpendicularly attached to the central copper ion, whereas the "relaxed" lowest excited state has a D_2 structure in which the dihedral angle (dha) between the two ligands is "flattened" to 65−75° (Figure 1). This structural difference between the ground and excited states is sometimes explained in relation to the structural difference between tetrahedral Cu(I) complexes and square planar Cu(II) complexes, because a d electron of the central copper ion is transferred to the ligands with metal-to-ligand

Received: September 24, 2010
Published: April 27, 2011

dx.doi.org/10.1021/ja108645x | J. Am. Chem. Soc. 2011, 133, 7728–7736

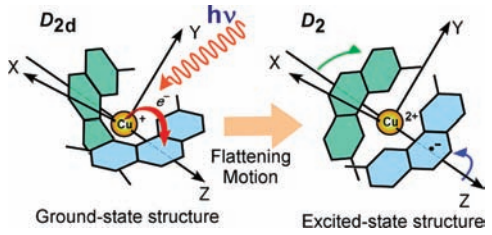

Figure 1. Photoinduced flattening distortion of $[Cu(dmphen)_2]^+$ in the MLCT excited state.

charge transfer (MLCT) excitation and the central copper is formally oxidized from Cu(I) to Cu(II). The structural change induced by the MLCT excitation has been supported by quantum chemical calculations[8,29−32] and a recent time-resolved X-ray experiment for the ^{3}MLCT state.[8]

Because the structural change of $[Cu(dmphen)_2]^+$ is triggered by MLCT photoexcitation, real-time observation of the relevant dynamics is possible with the use of ultrafast spectroscopy.[8,33−37] So far, several groups have studied the ultrafast dynamics of this complex using time-resolved absorption and emission spectroscopy.[8,31,33,34] Although there was an initial controversy on the interpretation of the observed dynamics,[8,31] we recently clarified the overall relaxation processes after $S_2 \leftarrow S_0$ photoexcitation using femtosecond time-resolved emission spectroscopy.[7] It was revealed that the initially populated S_2 state is relaxed mainly to the S_1 state retaining the perpendicular structure with ∼45 fs, and the $D_{2d} \rightarrow D_2$ structural change (the flattening distortion) occurs in the S_1 state with ∼660 fs. The intersystem crossing from the S_1 state to the T_1 state takes place after the structural change with a time constant of ∼7.4 ps. This time-resolved emission study not only clarified the kinetics of the relaxation processes but also shed new light on the mechanism of the structural change. Unexpectedly, the fluorescence spectral change accompanying the structural change exhibited an isoemissive point, indicating that the "well-defined" perpendicular S_1 state appears for a short finite period before the structural change. This finding does not accord with the structural change due to the ordinary (pseudo-) Jahn−Teller effect, because in such a case, the distortion is induced by the spontaneous structural instability at the perpendicular structure.[38−40] In this sense, the femtosecond time-resolved emission study indicated that the mechanism of the structural change of the metal complex is not as simple as had been believed.

In this paper, we report an ultrafast transient absorption study of $[Cu(dmphen)_2]^+$ in solution, which provides detailed information about the potential energy surface, related ultrafast dynamics, and vibrational structure of S_1 $[Cu(dmphen)_2]^+$. The experiment was carried out with time resolution as high as 30 fs, which allowed us not only to examine ultrafast relaxation dynamics but also to observe coherent nuclear wavepacket motion in the ^{1}MLCT state. Real-time observation of the excited-state nuclear motion provides crucial information about the S_1 potential energy surface that governs the structural change.[41] Ultrafast spectroscopy with complementary quantum chemical calculations successfully clarified the overall picture of the ultrafast structural change of the prototype metal complex, including its initial coherent nuclear dynamics.

EXPERIMENTAL SECTION

Materials. $[Cu(dmphen)_2]PF_6$ was prepared by the method reported in the literature.[42] The purity of the sample was checked by elemental analysis and absorption spectra. Dichloromethane (Wako, HPLC-grade) was used as received. A fresh sample solution was prepared for each time-resolved measurement. Absorption spectra of the sample were measured before and after the measurements, and no noticeable change was recognized.

Steady-State Measurements. Steady-state absorption spectra were recorded on a commercial spectrometer (U-3310, Hitachi).

Two-Color Pump−Probe Measurements with 30 fs Time Resolution. The experimental setup for two-color pump−probe measurements with 30-fs time resolution was previously described in detail.[19] Briefly, the light source was two home-built noncollinear optical parametric amplifiers (NOPAs) that were driven by the output of a Ti:sapphire regenerative amplifier (Legend Elite, Coherent, 800 nm, 1 kHz, 1 mJ, 80 fs).[19] The output of the first NOPA was used as the pump pulse (540 nm, 17 fs). The output of the second NOPA (650 nm, 16 fs) was divided into two, and they were used as the probe and reference pulses for monitoring the time-resolved absorption signals. The pump and probe pulses were focused into a 200-μm-thick flow cell of the sample solution. The intensities of the probe and reference pulses were detected by photodiodes, and the signals were processed on a shot-to-shot basis to evaluate the pump-induced absorbance change. The pump polarization was rotated by a half-wave plate to achieve the magic-angle condition. The time resolution of the measurement was 30 fs (full width at half-maximum, fwhm), which was determined by cross-correlation measurements of the pump and probe pulses with a 50-μm-thick BBO (β-barium borate) crystal.

Measurements of Transient Absorption Spectra with 200 fs Time Resolution. Time-resolved absorption spectra were measured with 200-fs time resolution. The light source of the apparatus was a Ti:sapphire regenerative amplifier (Legend, Coherent, 800 nm, 1 kHz). The amplified pulse was converted to a near-infrared pulse (1760 nm) with an optical parametric amplifier (TOPAS, Quantronix), and it was sum-frequency mixed with the fundamental pulse (800 nm) to generate a 550-nm pulse. This 550-nm pulse was used as the pump pulse for photoexcitation of the sample. A white-light continuum was generated by focusing a small fraction of the 800-nm pulse into a sapphire plate, and it was used as the probe and reference pulses. The sample solution was circulated through a 50-μm-thick jet nozzle. Probe and reference spectra of each five laser shots were measured with a spectrograph (500is/sm, Chromex) and a charge-coupled device (CCD; TEA/CCD-1024-EM/1 UV, Princeton instruments) that was read out at 100 Hz repetition rate. The effect of the chirp of the white-light probe on the time-resolved spectra was corrected on the basis of the OKE (optical Kerr effect) data of a thin glass plate, which were measured with the same experimental configuration.[43]

Quantum Chemical Calculations. The quantum chemical calculations for the ground and excited states of $[Cu(dmphen)_2]^+$ were carried out with density functional theory (DFT) and the time-dependent density functional theory (TDDFT), respectively, using the Becke three-parameter/Lee−Yang−Parr (B3LYP) functional. The basis sets used were STO-3G (H atom), double-ζ basis set[44] (C and N atoms), and cc-pVDZ-PP basis set[45] put on the effective core potential (ECP10MDF) (Cu atom).[46] The program used was Turbomole, a program package for ab initio electronic structure calculations.[47] The computations were performed at Research Center for Computational Science, Okazaki, Japan. In the calculation of potential curves along the dihedral angle of the two ligands (dha), the nitrogen atoms in the ligands were kept in the plane for which dha was defined, and all other degrees of freedom were optimized while D_2 symmetry was kept. The structures at the global and local potential minima of the potential energy surfaces were optimized, including dha, in the D_2 symmetry. The self-consistent field (SCF) energy convergence criterion of the present calculation was set at 2.7×10^{-6} eV for dha = 90.0° ± 1.0° in the S_1 state and 2.7×10^{-5} eV for the other points. At the local and global potential minima, normal-mode analysis was performed. In both the S_1 and S_0 states, the perpendicular structures with D_{2d} symmetry (dha = 90°) have no imaginary frequency, assuring that they are the true local/global minima.

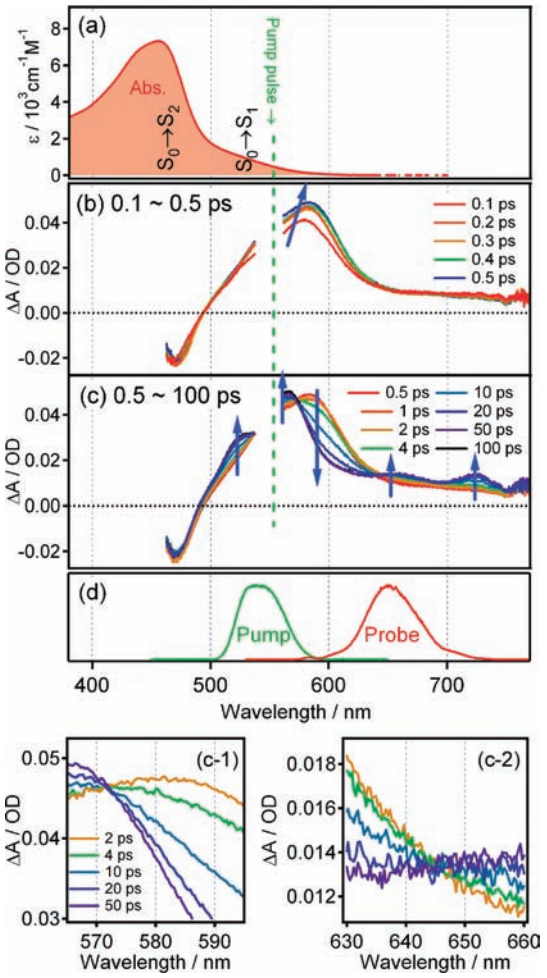

Figure 2. (a) Steady-state absorption spectrum of $[Cu(dmphen)_2]^+$ in dichloromethane. (b, c) Time-resolved absorption spectra of $[Cu(dmphen)_2]^+$ in dichloromethane in the delay time range of (b) 0.1−0.5 ps and (c) 0.5−100 ps. (Pump 550 nm; 7×10^{-2} mol·dm^{-3}.) (d) Spectra of the pump and probe pulses used for two-color pump−probe measurements. (c-1, c-2) Expanded views of panel c to clearly show the isosbestic points.

The flattened S_1 structure within D_2 symmetry (dha = 68°) has four imaginary frequencies, which correspond to the rotations of the four methyl groups. The true global minimum in the S_1 state has C_2 symmetry, in which the four methyl groups are slightly rotated from the D_2 structure. Details about the optimized structures are given in the Supporting Information.

RESULTS AND DISCUSSION

Steady-State and Femtosecond Time-Resolved Absorption Spectra. Figure 2a depicts the absorption spectrum of $[Cu(dmphen)_2]^+$ in the visible region, which exhibits two bands around ~460 and ~550 nm. Both the bands are assigned to MLCT transitions,[26,48−50] and we call the intense higher-energy transition (~460 nm) the $S_2 \leftarrow S_0$ transition and the weak lower-energy transition (~550 nm) the $S_1 \leftarrow S_0$ transition hereafter. In the perpendicular ground state of $[Cu(dmphen)_2]^+$ at the D_{2d} geometry, the highest occupied molecular orbitals (HOMO) are essentially degenerate d_{xz} and d_{yz} orbitals that have E symmetry, and the lowest unoccupied molecular orbitals (LUMO) are π^* orbitals of the two ligands, which also have E symmetry.[48−50] (See Figure 1 for the definition of the coordinate system.) In the MLCT configuration, one electron is transferred from HOMO to LUMO, and four nondegenerate electronic states are generated from the direct product of $E \otimes E = A_2 \oplus B_2 \oplus A_1 \oplus B_1$. Among them, only the B_2 state is optically allowed at the D_{2d} geometry, and the S_2 state showing an intense absorption band is assigned to the B_2 state. The S_1 state is assignable to the optically forbidden A_2 state that gains transition intensity by the effect of nuclear displacement. In the framework of the vibronic state of a D_{2d} molecule, the $A_2 \leftarrow A_1$ (ground-state) transition gains transition intensity by b_1 vibrations through vibronic coupling with the optically allowed $B_2 \leftarrow A_1$ transitions ($A_2 \otimes b_1 = B_2$). From the viewpoint of the static/dynamic flattening distortion, the very shallow S_0 potential curve along the relevant nuclear displacement (b_1 symmetry) gives rise to a substantial contribution from the distorted D_2 structure, which induces sizable oscillator strength by changing the optically forbidden A_2 state at D_{2d} to an optically allowed B_1 state of the distorted D_2 geometry.[51] Experimentally, the assignment of the S_1 state was made on the basis of the facts that the $S_1 \leftarrow S_0$ transition shows the same Z-polarization as the $S_2 \leftarrow S_0$ transition at 77 K and that the copper complexes, having more distorted structure, exhibit more intense $S_1 \leftarrow S_0$ transitions.[48] Recent TDDFT calculations also supported this assignment.[30−32]

Before performing two-color pump−probe measurements with 30-fs time resolution, we carried out spectral measurements of time-resolved absorption using white light continuum as the probe. The time resolution is moderate (~200 fs), but we can clarify the overall spectral change of transient absorption with this experiment. Although time-resolved absorption spectra of $[Cu(dmphen)_2]^+$ measured with $S_2 \leftarrow S_0$ excitation have already been reported,[8,35] the relaxation process of the S_2 state made the observation complicated and made it difficult to distinguish the dynamics of the structural change from the internal conversion and intersystem crossing. This problem led to erroneous interpretations in previous works (vide infra). In this work, in contrast, we excited the complex directly to the S_1 state, which made the spectral change simple and the interpretation straightforward.

Figure 2b and 2c show time-resolved absorption spectra obtained with $S_1 \leftarrow S_0$ excitation at 550 nm. Immediately after photoexcitation, an intense transient absorption peaked at 580 nm appeared with a broader and weaker tail extending to the wavelength region longer than 700 nm. A small intensity increase as well as a small red shift of the absorption maximum (580 → 585 nm) was observed in the subpicosecond time region (Figure 2b). Then, a new transient absorption band peaking around 565 nm appeared in accordance with the decay of the 585-nm band in the early picosecond time region up to 20 ps (Figure 2c). The 565-nm transient also exhibits additional peaks at 525, 660, and 725 nm. Note that clear isosbestic points were observed at 572 and 643 nm during this spectral change in the picosecond region (Figure 2, panels c-1 and c-2). The transient absorption spectra did not show any further change after 50 ps within the measured time range up to 100 ps.

We carried out global fitting analysis using multiexponential functions and found that the observed spectral changes were well reproduced with three components having time constants of 920 fs, 9.8 ps, and a very long one that could not be determined within the delay time range measured. In our previous time-resolved emission study,[7] we clarified the following dynamics occurring after S_2 excitation, on the basis of quantitative analysis on the spectra, lifetimes, and radiative lifetimes (oscillator strength) of

the transients:

$$S_0^{perp} \xrightarrow{h\nu} S_2^{perp}\ (45\ fs) \xrightarrow{IC}$$

$$S_1^{perp}\ (660\ fs) \xrightarrow[\text{distortion}]{\text{structural}} S_1^{flattened}\ (7.4\ ps) \xrightarrow{ISC} T_1^{flattened} \rightarrow$$

where the superscripts denote the structure of each excited state (i.e., perp = perpendicular structure; flattened = flattened structure) and the number in parentheses is the lifetime of each transient. Because the complex is directly excited to the S_1 state in the present experiment, we observe the dynamics starting from the perpendicular S_1 state (S_1^{perp}). Therefore, the 920-fs and 9.8-ps dynamics observed in the transient absorption are straightforwardly attributed to decays of the perpendicular S_1 state ($S_1^{perp} \rightarrow S_1^{flattened}$) and flattened S_1 state ($S_1^{flattened} \rightarrow T_1^{flattened}$), respectively. The longest time constant is assignable to the lifetime of the flattened T_1 state (41 ns).[7] It is noteworthy that the transient absorption change corresponding to the flattening distortion is small, although a very distinct change has been observed in the time-resolved fluorescence spectra.[7] The transient absorption spectra showed only a small intensity increase and a small red shift of the absorption maximum with the flattening distortion.

The lifetime of the perpendicular S_1 state (~920 fs) evaluated by the present transient absorption measurements is somewhat longer than that determined by our previous fluorescence up-conversion experiments (~660 fs).[7] There are two possible reasons for this deviation. First, the present transient absorption experiment was carried out with S_1 excitation, whereas the previous femtosecond fluorescence experiment was performed with S_2 excitation. This difference in initial photoexcitation causes a difference in the vibrational excess energy of the S_1 state generated, which may cause some change in the time constant of the structural change. Second, as already mentioned, the spectral change of the transient absorption due to the structural change is small, compared to that observed in the time-resolved fluorescence. Therefore, the time constant evaluated from the small transient absorption change may have a larger error. In spite of this deviation, however, it is safe to say that the lifetime of the perpendicular S_1 state is 700−900 fs.

In recent papers of Chen and co-workers,[35,52] it was claimed that the flattering distortion occurs with a time constant of ~100 fs on the basis of time-resolved fluorescence and absorption data obtained with S_2 excitation. In addition, they claimed that the faster $S_1 \rightarrow T_1$ intersystem crossing takes place at different structures while the flattening distortion is proceeding, in addition to the slow intersystem crossing occurring in the flattened S_1 state after distortion. Our transient absorption spectra measured with direct S_1 excitation clearly showed that the time constant of the structural change is 700−900 fs, as we concluded in our previous femtosecond fluorescence study.[7] Our results also indicate that faster $S_1 \rightarrow T_1$ intersystem crossing does not occur, or is negligible, while the structural change proceeds, at least in dichloromethane. In fact, in the time region when the structural change proceeds (~ 1 ps), any feature assignable to the T_1 state does not appear, which denies formation of the T_1 state in this time range. In addition, the spectral change in the later time (2−50 ps; Figure 2, panels c-1 and c-2) exhibits clear isosbestic points, demonstrating that this process is the conversion from a well-defined single precursor (the flattened S_1) to the product (the flattened T_1). Consequently, there was no indication of various T_1 states that are generated at different structures and undergo structural changes afterward. The present femtosecond time-resolved absorption data strongly confirmed that the time scales of the flattening distortion and the intersystem crossing are well separated in this complex, as concluded in our previous work. We note that the direct S_1 excitation realized in the present work is essential to obtain the clear conclusion about the ultrafast dynamics of $[Cu(dmphen)_2]^+$ based on femtosecond time-resolved absorption data. In the case of S_2 photoexcitation, a minor but substantial intersystem crossing occurs directly from the (perpendicular) S_2 state immediately after photoexcitation,[7] and hence the S_2 excitation generates a mixture of singlet and triplet states even before the structural change. This made the observed spectral change complicated and made it very difficult to unambiguously interpret the transient absorption data, which we think caused confusion in the previous works.[8,34,35,52] It may be worth mentioning that the solvent used in our studies (dichloromethane) is different from that used in the works of Chen and co-workers. Although it is known that some solvents, such as acetonitrile, coordinate to the flattened excited state whereas dichloromethane does not, the ultrafast process occurring in a few picoseconds is not affected because coordination is a rather slow process. Because the steady-state absorption spectra indicate that the ground-state structure, from which the ultrafast process starts with photoexcitation, is essentially the same in these solvents,[26] the conclusion obtained in the present experiments is also valid for the ultrafast dynamics in other solvents.

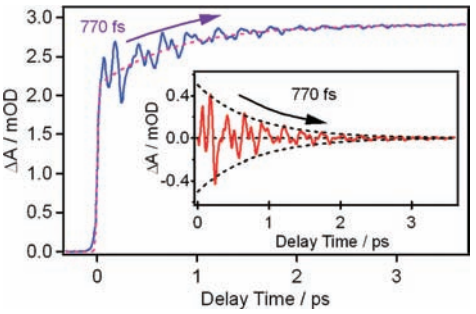

Figure 3. Time-resolved absorption signals of $[Cu(dmphen)_2]^+$ in dichloromethane. Pump 540 nm; probe 650 nm; 2.5×10^{-2} mol·dm^{-3}. (Inset) Oscillatory component of the time-resolved absorption signal (red line). Dashed lines are exponential fits drawn with a time constant of 770 fs.

Observation of Nuclear Wavepacket Motion by Ultrafast Pump−Probe Measurements. On the basis of the spectral information obtained by the femtosecond time-resolved absorption measurements, we carried out two-color pump−probe measurements with 30-fs time resolution. The spectra of the pump and probe pulses are shown in Figure 2d. The center wavelength of the pump pulse was tuned to 540 nm to excite the molecule directly to the S_1 state. The probe was set around 650 nm, where the transient absorption appears but the ground-state absorption is absent, to selectively observe the initial S_1 dynamics by monitoring the transient absorption of the S_1 state. Figure 3 depicts the time-resolved trace obtained by the pump−probe measurement. As seen in this figure, the transient absorption appeared instantaneously at the time origin, and then the intensity increase was observed in the subpicosecond time region. This rise was well-fitted with an exponential function with a time constant of 770 fs. This component corresponds to the 920-fs dynamics observed in the spectral measurement, which

dx.doi.org/10.1021/ja108645x | J. Am. Chem. Soc. 2011, 133, 7728–7736

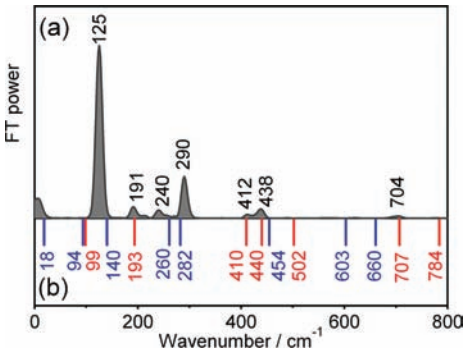

Figure 4. Low-frequency vibrational spectra of $[Cu(dmphen)_2]^+$ in the perpendicular S_1 state. (a) Fourier transform power spectrum of the oscillatory components (filled with gray). (b) Frequencies of the normal modes calculated by TDDFT (red, a_1 symmetry; blue, b_1 symmetry).

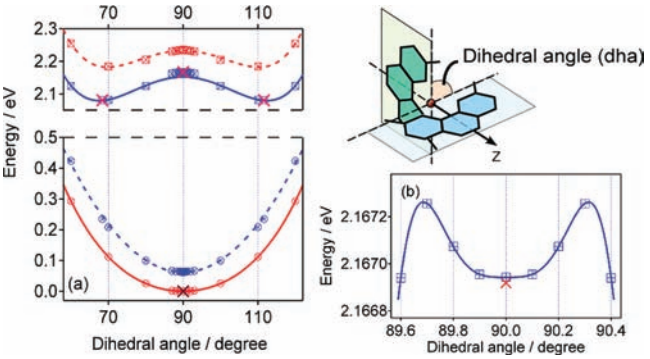

Figure 5. Results of DFT/TDDFT calculations for S_0 and S_1 states of $[Cu(dmphen)_2]^+$. (a) Potential energy curves of S_1 and S_0 states as a function of dihedral angle. Circles and squares are the calculated points, and the lines are fits with polynomials. Red circles and squares show energies of the S_0 and S_1 states, respectively, at the structures optimized for the S_0 state. Blue circles and squares show S_0 and S_1 energies at the structures optimized for the S_1 state. The calculation was made at each fixed dha, and geometry optimization was performed for other structural parameters. At the local minima indicated by the cross markers, the optimization including dha was carried out. (b) S_1 potential energy curve around dha = 90° (optimized for the S_1 state).

was assigned to the flattening distortion in the S_1 state. The probe tuned to 650 nm can detect the absorbance change in the 600−700 nm region because of its broad spectral bandwidth. The most characteristic feature of the pump−probe signal is a clear oscillation that starts at the time origin and lasts for a few picoseconds. This oscillatory component was extracted by use of the exponential function that was best-fitted to the slow population component (inset of Figure 3). The damping time of the oscillation was essentially the same as the time constant of the structural change (~770 fs). It implies that the oscillation arises from the coherent nuclear motion of the S_1 state before the structural change (S_1^{perp}) and that the coherence is damped as the structural change occurs. In other words, the lifetime of the vibrational coherence is determined by the population lifetime of the perpendicular S_1 state. This observation demonstrated that the perpendicular S_1 state generated by photoexcitation has a well-defined vibrational structure and can vibrate within its lifetime shorter than 1 ps. The S_1 state stays undistorted in a short period before the structural change.

Figure 4 depicts the power spectrum of the Fourier transform (FT spectrum) of the oscillation observed in the pump−probe measurement. A number of vibrational modes contribute to the oscillation, and the most prominent contribution arises from the 125-cm^{-1} vibration. This FT spectrum represents the vibrational spectrum of the perpendicular S_1 state (S_1^{perp}), which transiently appears in the subpicosecond region after $S_1 \leftarrow S_0$ photoexcitation.

Theoretical Calculation of Potential Energy Surfaces. We calculated the energies of the S_1 and S_0 states by DFT/TDDFT to associate the observation of ultrafast spectroscopy with relevant potential energy surfaces. Because the potential energy surface of $[Cu(dmphen)_2]^+$ has 165 [= (3 × 57) − 6] dimensions, we focused on the potential curves along the dihedral angle. The S_0 potential curve calculated by DFT is shown with a red solid line in Figure 5. This curve was obtained by calculating the S_0 energy at each dihedral angle with optimization of other structural parameters in the S_0 state. The S_1 energy at each structure on this S_0 potential curve was also calculated by TDDFT and is depicted with a red dashed line in the figure. The energy difference between the red solid line and red dashed line represents the $S_1 \leftarrow S_0$ transition energy at each S_0 structure. In a similar manner, the S_1 potential curve along the dihedral angle was calculated by TDDFT, and it is drawn with a blue solid line in Figure 5. This curve was obtained by calculating the S_1 energy at each dihedral angle by optimizing the other structural parameters in the S_1 state under the restriction of D_2 symmetry.

Table 1. Comparison of Calculated and Experimental S_1-S_0 Transition Energies of $[Cu(dmphen)_2]^+$

		S_1-S_0 transition energy (eV)	
structure	transition	calculation	experiment
perpendicular	$S_1 \leftarrow S_0$	2.24 (555 nm)	2.25[a] (550 nm)
perpendicular	$S_1 \rightarrow S_0$	2.11 (589 nm)	2.07[b] (600 nm)
flattened	$S_1 \rightarrow S_0$	1.85 (672 nm)	1.72[b] (720 nm)

[a] Transition energies were obtained from the peak position in the absorption spectrum. [b] Transition energies were obtained from the peak position in time-resolved fluorescence spectra reported in ref 7.

The S_0 energy at each structure on this S_1 potential curve was also calculated, and it is drawn with a blue dashed line. The energy difference between the blue solid line and blue dashed line represents $S_1 \rightarrow S_0$ transition energy at each S_1 structure. The global minima of the S_0 and S_1 potential energy surfaces appear at dha = 90° and dha = 68° (and 112°) on the S_0 and S_1 potential curves, respectively, which is consistent with the results of other groups.[8,30−32] (We note that the true global minimum of the S_1 potential ($S_1^{flattened}$) was found at a structure of C_2 symmetry which is very close to the D_2 flattened structure; see Supporting Information)

In Table 1, the transition energies calculated from the obtained S_1 and S_0 potential curves are compared with the experimental values. The $S_1 \leftarrow S_0$ transition energy at the perpendicular S_0 structure (i.e., energy difference between solid and dashed red lines at dha = 90°) was calculated at 2.24 eV, which agrees very well with the $S_1 \leftarrow S_0$ transition energy obtained from the absorption spectrum (2.25 eV). The $S_1 \rightarrow S_0$ transition energies (i.e., energy difference between solid and dashed blue lines) at dha = 90° and 68° were 2.11 and 1.85 eV, respectively, and they are also in fairly good agreement with the transition energies of the $S_1 \rightarrow S_0$ fluorescence before and after structural change (2.07 and 1.72 eV).[7] These agreements assure that the present computation well reproduces the potential energy surfaces of $[Cu(dmphen)_2]^+$.

dx.doi.org/10.1021/ja108645x | J. Am. Chem. Soc. 2011, 133, 7728–7736

The global minimum of the calculated S_0 potential energy surface is located at dha = 90°, which is consistent with the perpendicular structure of the S_0 state. The global minimum of the calculated S_1 potential energy surface is located at dha = 68° (112°), which rationalizes ultrafast structural change occurring in the S_1 state after photoexcitation. Moreover, as seen in the expanded view of the S_1 potential surface (Figure 5b), the DFT/TDDFT calculation showed that the potential around the perpendicular structure (dha = 90°) is very flat and even exhibits a shallow local minimum. The calculated depth of the minimum is much larger than the SCF energy convergence criterion of the present calculation (2.7×10^{-6} eV), assuring that the minimum is not an artifact of the calculation. The existence of this local minimum was also confirmed by normal-mode analysis (vide infra). This feature of the calculated S_1 potential curve accords with the result of ultrafast spectroscopy, which indicates that the perpendicular S_1 state appears before the flattening distortion.

A further discussion on the S_1 potential energy surface (e.g., a quantitative discussion on the depth of the local minimum at the perpendicular structure) is beyond the level of the present calculation. Nevertheless, it is crucially important that the DFT/TDDFT calculation indicated a very flat feature of the potential curve and even a local minimum at the perpendicular structure because it is not expected in the standard picture of (pseudo-) Jahn−Teller effect, which has been accepted as the mechanism of the photoinduced structural change of the metal complex. The result of the quantum chemical calculation confirms that the realistic mechanism of the photoinduced structural change is not so simple as was believed before our work.

The Jahn−Teller distortion is discussed on the basis of the following expansion of the potential curve of the relevant electronic state with respect to a nuclear coordinate:[38−40]

$$E(Q) = E_1 + \left\langle \psi_1 \left| \frac{\partial \hat{H}}{\partial Q} \right| \psi_1 \right\rangle Q + \left(\frac{1}{2} \left\langle \psi_1 \left| \frac{\partial^2 \hat{H}}{\partial Q^2} \right| \psi_1 \right\rangle + \sum_{n \neq 1} \frac{\left| \left\langle \psi_n \left| \frac{\partial \hat{H}}{\partial Q} \right| \psi_1 \right\rangle \right|^2}{E_1 - E_n} \right) Q^2 \quad (1)$$

$$= E_1 + f_1 Q + f_2 Q^2 \quad (2)$$

where $\hat{H}$ and ψ_1 denote the Hamiltonian and wave function of the molecule in the S_1 state. In the case of the ^{1}MLCT state of $[Cu(dmphen)_2]^+$, the second term (which is the origin of the first-order Jahn−Teller effect) vanishes for non-totally symmetric vibrations because the S_1 state has the nondegenerate A_2 symmetry. The structural stability of the perpendicular S_1 state is discussed for the quadratic Q^2 terms, which determine the curvature of the potential curve at the $Q = 0$ geometry. The sign of the curvature is determined by the relative magnitude of the two terms in the quadratic Q^2 term. If the balance of the two terms makes the f_2 value negative ($f_2 < 0$), the potential curve exhibits a parabolic feature opening downward, giving rise to structural instability at the $Q = 0$ geometry (pseudo-Jahn−Teller effect or second-order Jahn−Teller effect). On the other hand, when the f_2 value is greater than zero ($f_2 > 0$), the potential curve has a parabolic feature opening upward and a local minimum appears in the potential curve at the $Q = 0$ geometry. The present DFT/TDDFT calculation carried out a realistic evaluation of the f_2 value at the perpendicular geometry and showed that the f_2 value is actually not negative. The potential energy surface is very flat and it has a parabolic form opening a little upward at the perpendicular structure. Thus, the S_1 state stays undistorted for a short time as observed in the ultrafast pump−probe experiment. The calculated potential energy curves strongly support the new picture of photoinduced structural change of $[Cu(dmphen)_2]^+$.[7]

It is worth noting that it is not adequate to simply correlate the calculated low potential barrier in the S_1 state to the observed lifetime of the perpendicular S_1 state, in a traditional sense based on transition-state theory. In transition-state theory, it is assumed that the reactant is thermally equilibrated and is in equilibrium with the transition state. Then, the reaction rate is connected to the energy barrier of the reaction (i.e., the energy difference between the reactant and transition state). In this picture, we can say that the molecule stays on the reactant side "statistically" for a certain period before the reaction. On the other hand, in extremely fast reactions, the excited state generated by photoexcitation (i.e., the reactant) is highly unequilibrated and its dynamics needs be treated directly with the trajectories of the nuclear wavepacket on the excited-state potential energy surface. In this view, it is natural to think that it takes a finite time for molecule to escape from the region where the excited state is initially generated, even if the potential is very flat and the energy barrier is low. Because the nuclear wavepacket can oscillate along the coordinates perpendicular to the reaction coordinate, we may say that the molecule "dynamically" stays on the reactant side in this case. Because the structural change of $[Cu(dmphen)_2]^+$ proceeds in the S_1 state with a femtosecond time scale, it should be categorized to the latter case, or at least it has some character of the latter category. Because this is an essential issue for proper understanding of ultrafast chemical reactions, it is highly desirable to compare the observed dynamics with a molecular dynamics simulation on the S_1 potential energy surface, although it is beyond the scope of the present study.

Assignment of Coherent Nuclear Wavepacket Motion in the S_1 State. To clarify the initial nuclear dynamics of the photoinduced structural change, we performed a normal coordinate analysis of the perpendicular S_1 state calculated by TDDFT. We first focused on the totally symmetric vibrations (a_1) because, in usual cases, the nuclear wavepacket motions due to a_1 vibrations appear in the ultrafast pump−probe measurements through the Franck−Condon mechanism.[17−19,41,53−55] The frequencies of totally symmetric vibrations calculated in the 0−800 cm^{-1} region are shown with red bars in Figure 4 and are compared with the FT spectrum of the oscillation observed in the pump−probe measurement. As is readily seen, most of the observed coherent motion is assignable to the a_1 mode: The vibrations observed at 125, 191, 412, 438, and 704 cm^{-1} are assignable to the calculated frequencies of 99, 193, 410, 440, and 707 cm^{-1}, respectively. A common character of the assigned a_1 modes is that they contain substantial change of the Cu−N bond lengths. As an example, the vibrational mode assigned to the most intense 125-cm^{-1} band is depicted in Figure 6a. (See Figure S1 in Supporting Information for the other modes.) This 125-cm^{-1} vibration is the "breathing" mode of the complex, which is induced by the symmetric stretching of the Cu−N bond. The appearance of these a_1 modes is readily rationalized by the structural change induced by photoexcitation. In fact, the substantial shortening of the Cu−N bonds is expected with MLCT excitation because HOMO of the S_0 state has some antibonding character for

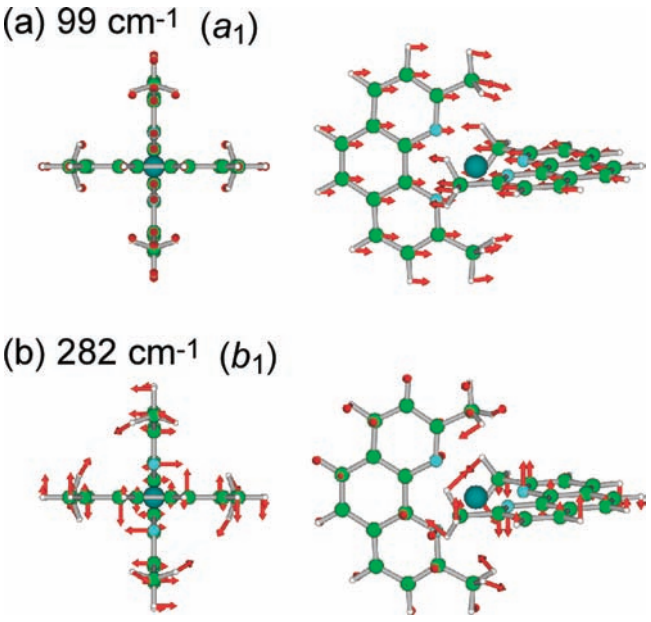

Figure 6. Vibrational modes of the perpendicular S_1 state of $[Cu(dmphen)_2]^+$ calculated at (a) 99 and (b) 282 cm^{-1}. The displacement vector of each atom is depicted by red arrows.

the Cu−N bonds.[31] In addition, the electrostatic attraction between the ligands and metal center increases in the MLCT excited state, which also contributes to the shortening of the Cu−N bonds. This shortening of the Cu−N bonds is supported by computation and experiment. The present DFT/TDDFT calculated the Cu−N bond length in the perpendicular S_1 state to be shorter than that of the S_0 state by 0.011 Å. It has been reported that the vibrational modes having the Cu−N stretch motion appear in the resonance Raman spectrum of $[Cu(dmphen)_2]^+$, which also indicates that the Cu−N bond length is changed upon $S_1 \leftarrow S_0$ excitation.[56] As the Cu−N bond length is substantially changed with $S_1 \leftarrow S_0$ excitation, it is natural that the coherent nuclear motion containing the Cu−N stretch motion is induced in the S_1 state with photoexcitation.

Interestingly, there was no a_1 mode assignable to the 290-cm^{-1} component that gives the second largest contribution to the nuclear wavepacket motion observed. As already mentioned, the $S_1 \leftarrow S_0$ transition gains its intensity through vibronic coupling with the S_2 state that exhibits strong absorption around 460 nm. Because the S_1 (A_2) state is coupled with the S_2 (B_2) states through the b_1 vibration, the b_1 mode can be excited with the $S_1 \leftarrow S_0$ excitation through vibronic coupling. Using TDDFT, we evaluated the magnitude of the S_1-S_2 vibronic coupling induced by each b_1 mode and found that the coupling is realized mainly by the ν_{25} mode calculated at 282 cm^{-1} (see Supporting Information). Therefore, we assigned the 290 cm^{-1} band in the FT spectrum to the ν_{25} mode having b_1 symmetry. As depicted in Figure 6b, the ν_{25} mode is ascribed to the twisting motion of the ligands of the complex. This mode induces large displacements of the ligand atoms that face the central copper, which efficiently mixes the S_1 and S_2 states having different MLCT characters. It is noteworthy that the flattening motion also has b_1 symmetry. (The frequency of the flattening motion was calculated to be 18 cm^{-1} for the perpendicular S_1 state.) Because the motions having the same symmetry can be coupled with anharmonicity, we can expect an efficient energy flow from the coherently excited ligand twisting vibration to the flattening motion. In this sense, the coherent nuclear motion along the ligand twisting coordinate may promote the flattening distortion of the perpendicular S_1 state.

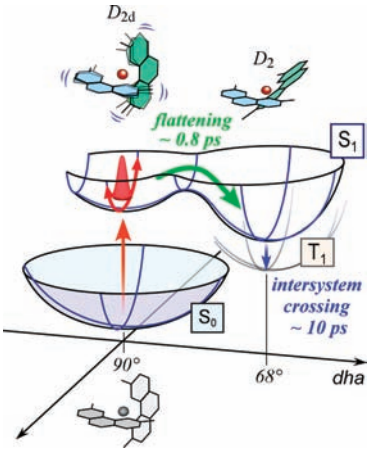

Figure 7. Schematic diagram of the mechanism of photoinduced structural change of $[Cu(dmphen)_2]^+$.

Mechanism of Photoinduced Structural Change of $[Cu(dmphen)_2]^+$. Ultrafast spectroscopy and complementary quantum chemical calculation has disclosed the mechanism and dynamics of photoinduced structural change of $[Cu(dmphen)_2]^+$ as sketched in Figure 7. The S_0 state has the perpendicular D_{2d} structure, so that the $S_1 \leftarrow S_0$ photoexcitation initially generates the perpendicular S_1 state. The S_1 potential energy surface around the perpendicular structure is very flat and highly likely has a shallow local minimum, so that the S_1 state retains the perpendicular geometry for a short finite time. The distinct coherent nuclear motion due to a_1 modes and a b_1 mode is induced in the S_1 state with photoexcitation. The S_1 state leaves the perpendicular geometry with a time constant of ~800 fs, and it is relaxed to the flattened structure with losing coherence of the nuclear motion. An efficient energy flow may occur from the coherent ligand-twisting vibration to the flattening motion through the anharmonic coupling. The intersystem crossing takes place predominantly in the flattened S_1 state with a time constant of ~10 ps. The long-lived flattened T_1 state is generated, and the well-known red-shifted phosphorescence is emitted.

The present work clarified the ultrafast dynamics of a prototypical metal complex $[Cu(dmphen)_2]^+$ with solid and clear spectroscopic observations. It was shown that the structural change and the intersystem crossing occur in the lowest ^{1}MLCT state with time constants of ~800 fs and ~10 ps, respectively, and that the time scales of the two processes are well-separated. Observation of the excited-state coherent nuclear motion, as well as the result of TDDFT calculation, strongly indicated that the S_1 state at the perpendicular geometry appears as a well-defined precursor before the structural change. Because this conclusion contradicts the picture based on the ordinary pseudo-Jahn−Teller effect, the present results request essential change of the mechanism accepted so far. In this sense, this work not only clarified the overall ultrafast dynamics of the prototypical complex but also provided a new paradigm for the photoinduced structural change of the metal complex. We note that ultrafast spectroscopy is highly capable of elucidating details of the photochemical process of metal complexes,[4−8,10−12,22,24,52,57−60] which has not been well clarified compared with the process of organic compounds. The solid and deep understanding provided by ultrafast spectroscopy

dx.doi.org/10.1021/ja108645x | J. Am. Chem. Soc. 2011, 133, 7728–7736

forms a firm basis to fully make use of metal complexes in a variety of applications.

■ ASSOCIATED CONTENT

Supporting Information. It provides following materials: tables for vibrational frequencies of $[Cu(dmphen)_2]^+$; figures for a_1 and b_1 vibrational modes of $[Cu(dmphen)_2]^+$; text for estimation of vibronic coupling between S_1 (A_2) and S_2 (B_2) states; and details of quantum chemical calculations for optimized structures at local and global minima on S_1 and S_0 potential energy surfaces. This material is available free of charge via the Internet at http://pubs.acs.org.

■ AUTHOR INFORMATION

Corresponding Author

*Telephone +81-48-467-4592; fax +81-48-467-4539; e-mail tahei@riken.jp.

Present Addresses

†Department of Chemistry, University of Toyama, 3190 Gofuku, Toyama 930-8555, Japan.

‡Department of Theoretical and Computational Molecular Science, Institute for Molecular Science, 38 Nishigo-Naka, Myodaiji, Okazaki, 444-8585, Japan.

■ ACKNOWLEDGMENT

This work was supported by a Grant-in-Aid for Scientific Research on Priority Area "Molecular Science for Supra Functional Systems" (19056009) from MEXT and Grant-in-Aid for Scientific Research (A) (22245005) from JSPS.

■ REFERENCES

(1) Cotton, F. A.; Wilkinson, G. *Advanced Inorganic Chemistry*; Wiley: New York, 1980.
(2) Kalyanasundaram, K. *Photochemistry of polypyridine and porphyrin complexes*; Academic Press: London, 1992.
(3) Balzani, V.; Campagna, C. *Coordination Compounds I*; Springer: Berlin, 2007.
(4) Damrauer, N. H.; Cerullo, G.; Yeh, A.; Boussie, T. R.; Shank, C. V.; McCusker, J. K. *Science* **1997**, *275*, 54.
(5) Yeh, A. T.; Shank, C. V.; McCusker, J. K. *Science* **2000**, *289*, 935.
(6) Huse, N.; Kim, T. K.; Jamula, L.; McCusker, J. K.; de Groot, F. M. F.; Schoenlein, R. W. *J. Am. Chem. Soc.* **2010**, *132*, 6809.
(7) Iwamura, M.; Takeuchi, S.; Tahara, T. *J. Am. Chem. Soc.* **2007**, *129*, 5248.
(8) Chen, L. X.; Shaw, G. B.; Novozhilova, I.; Liu, T.; Jennings, G.; Attenkofer, K.; Meyer, G. J.; Coppens, P. *J. Am. Chem. Soc.* **2003**, *125*, 7022.
(9) Smolentsev, G.; Soldatov, A. V.; Chen, L. X. *J. Phys. Chem. A* **2008**, *112*, 5363.
(10) Cannizzo, A.; Mourik, F. v.; Gawelda, W.; Zgrablic, G.; Bressler, C.; Chergui, M. *Angew. Chem., Int. Ed.* **2006**, *45*, 3714.
(11) Gawelda, W.; Johnson, M.; de Groot, F. M. F.; Abela, R.; Bressler, C.; Chergui, M. *J. Am. Chem. Soc.* **2006**, *128*, 5001.
(12) Bressler, C.; Milne, C.; Pham, V. T.; ElNahhas, A.; van der Veen, R. M.; Gawelda, W.; Johnson, S.; Beaud, P.; Grolimund, D.; Kaiser, M.; Borca, C. N.; Ingold, G.; Abela, R.; Chergui, M. *Science* **2009**, *323*, 489.
(13) Daniel, C. *Coord. Chem. Rev.* **2003**, *238*, 143.
(14) Balzani, V.; Credi, A.; Raymo, F., M.; Stoddart, J. F. *Angew. Chem., Int. Ed.* **2000**, *39*, 3348.
(15) Sato, O. *Acc. Chem. Res.* **2003**, *36*, 692.
(16) Nishihara, H. *Bull. Chem. Soc. Jpn.* **2004**, *77*, 407.
(17) Takeuchi, S.; Tahara, T. *J. Chem. Phys.* **2004**, *120*, 4768.
(18) Ishii, K.; Takeuchi, S.; Tahara, T. *Chem. Phys. Lett.* **2004**, *398*, 400.
(19) Takeuchi, S.; Tahara, T. *J. Phys. Chem. A* **2005**, *109*, 10199.
(20) Tahara, T.; Takeuchi, S.; Ishii, K. *J. Chin. Chem. Soc.* **2006**, *53*, 181.
(21) Iwamura, M.; Watanabe, H.; Ishii, K.; Takeuchi, S.; Tahara, T. In *Ultrafast Phenomena XVI*; Springer Series in Chemical Physics; Springer: Berlin, 2009; Vol. 92, p 382.
(22) Consani, C.; Prémont-Schwarz, M.; ElNahhas, A.; Bressler, C.; Mourik, F. v.; Cannizzo, A.; Chergui, M. *Angew. Chem., Int. Ed.* **2009**, *48*, 7184.
(23) van der Veen, R. M.; Cannizzo, A.; van Mourik, F.; Vlček, A., Jr.; Chergui, M. *J. Am. Chem. Soc.* **2010**, *133*, 305.
(24) Schrauben, J. N.; Dillman, K. L.; Beck, W. F.; McCusker, J. K. *Chem. Sci.* **2010**, *1*, 405.
(25) Armaroli, N. *Chem. Soc. Rev.* **2001**, *30*, 113.
(26) Scaltrito, D. V.; Thompson, D. W.; O'Callaghan, J. A.; Meyer, G. J. *Coord. Chem. Rev.* **2000**, *208*, 243.
(27) Cunningham, C. T.; Moore, J. J.; Cunningham, K. L. H.; Fanwick, P. E.; McMillin, D. R. *Inorg. Chem.* **2000**, *39*, 3638.
(28) Lavie-Cambot, A.; Cantuela, M.; Leydet, Y.; Jonusauskas, G.; Bassania, D. M.; McClenaghana, N. D. *Coord. Chem. Rev.* **2008**, *252*, 2572.
(29) Shinozaki, K.; Kaizu, Y. *Bull. Chem. Soc. Jpn.* **1994**, *67*, 2435.
(30) Zgierski, M. Z. *J. Chem. Phys.* **2003**, *118*, 4045.
(31) Siddique, Z. A.; Yamamoto, Y.; Ohno, T.; Nozaki, K. *Inorg. Chem.* **2003**, *42*, 6366.
(32) Wang, X.; Lv, C.; Koyama, M.; Kubo, M.; Miyamoto, A. *J. Organomet. Chem.* **2005**, *691*, 551.
(33) Samia, A. C. S.; Cody, J.; Fahrni, C. J.; Burda, C. *J. Phys. Chem. B* **2004**, *108*, 563.
(34) Gunaratne, T.; Rodgers, M. A. J.; Felder, D.; Nierngarten, J.-F.; Accorsi, G.; Armaroli, N. *Chem. Commun.* **2003**, 3010.
(35) Shaw, G. B.; Grant, C. D.; Shirota, H.; Castner, E. W., Jr.; Meyer, G. J.; Chen, L. X. *J. Am. Chem. Soc.* **2007**, *129*, 2147.
(36) Nakashima, S.; Nagasawa, Y.; Seike, K.; Okada, T.; Sato, M.; Kohzuma, T. *Chem. Phys. Lett.* **2000**, *331*, 396.
(37) Cimei, T.; Bizzarri, A. R.; Cannistraro, S.; Cerullo, G.; Silvestri, S. D. *Chem. Phys. Lett.* **2002**, *362*, 497.
(38) Jahn, H. A.; Teller, E. *Proc. R. Soc. London* **1937**, *161A*, 220.
(39) Person, R. G. *Proc. Natl. Acad. Sci. U.S.A.* **1975**, *72*, 2104.
(40) Person, R. G. *J. Mol. Struct.* **1983**, *103*, 25.
(41) Takeuchi, S.; Ruhman, S.; Tsuneda, T.; Chiba, M.; Taketsugu, T.; Tahara, T. *Science* **2008**, *322*, 1073.
(42) McMillin, D. R.; Buckner, M. T.; Ahn, B. T. *Inorg. Chem.* **1977**, *16*, 943.
(43) Yamaguchi, S.; Hamaguchi, H. *Appl. Spectrosc.* **1995**, *49*, 1381.
(44) Schaefer, A.; Horn, H.; Ahlrichs., R. *J. Chem. Phys.* **1992**, *97*, 2571.
(45) Peterson, K. A.; Puzzarini, C. *Theor. Chem. Acc.* **2005**, *114*, 283.
(46) Figgen, D.; Rauhut, G.; Dolg, M.; Stoll, H. *Chem. Phys.* **2005**, *311*, 227.
(47) Boecker, S.; Deglmann, P.; Furche, F.; Haeser, M. *Turbomole, v 5-9-1*; University of Karlsruhe, Germany, 2007.
(48) Parker, W. L.; Crosby, G. A. *J. Phys. Chem.* **1989**, *93*, 5692.
(49) Everly, R. M.; McMillin, D. R. *J . Phys. Chem.* **1991**, *95*, 9071.
(50) McMillin, D. R.; McNett, K. M. *Chem. Rev.* **1998**, *98*, 1201.
(51) Keeping this effect of the nuclear displacement in our mind, we treat the geometry of the S_0 state as D_{2d} in this paper.
(52) Chen, L. X.; Zhang, X. Y.; Lockard, J. V.; Stickrath, A. B.; Attenkofer, K.; Jennings, G.; Liu, D. J. *Acta Crystallogr., Sect. A* **2010**, *66*, 240.
(53) Ishii, K.; Takeuchi, S.; Tahara, T. *J. Chem. Phys.* **2009**, *131*, 044512.
(54) Ishii, K.; Takeuchi, S.; Tahara, T. *J. Phys. Chem. A* **2008**, *112*, 2219.

(55) Although the $S_1 \leftarrow S_0$ transition of $[Cu(dmphen)_2]^+$ is optically forbidden at the exact perpendicular D_{2d} geometry, the a_1 nuclear wavepacket motion can be induced on the "false origin" of a b_1 vibrational level and/or through the static/dynamic flattening distortion due to the very shallow S_0 potential curve along the relevant nuclear displacement.

(56) Lind, S. J.; Gordon, K. C.; Waterland, M. R. *J. Raman Spectrosc.* **2008**, *39*, 1556.

(57) Bhasikuttan, A. C.; Suzuki, M.; Nakashima, S.; Okada, T. *J. Am. Chem. Soc.* **2002**, *124*, 8398.

(58) Wallin, S.; Davidsson, J.; Modin, J.; Hammarstrom, L. *J. Phys. Chem. A* **2005**, *109*, 4697.

(59) Juban, E. A.; Smeigh, A. L.; Monat, J. E.; McCusker, J. K. *Coord. Chem. Rev.* **2006**, *250*, 1783.

(60) Sugita, A.; Saito, T.; Kano, H.; Yamashita, M.; Kobayashi, T. *Phys. Rev. Lett.* **2001**, *86*, 2158.